Engineering Structures 114 (2016) 226–240

Contents lists available at ScienceDirect

Engineering Structures

journal homepage: www.elsevier.com/locate/engstruct

Investigation of a new experimental method for damage assessment of RC beams failing in shear using piezoelectric transducers

Maristella E. Voutetaki [a,*], Nikos A. Papadopoulos [b], Georgia M. Angeli [b], Costas P. Providakis [a]

[a] School of Architectural Engineering, Technical University of Crete, Chania 73100, Greece
[b] Department of Civil Engineering, Democritus University of Thrace, Xanthi 67100, Greece

ARTICLE INFO

Article history:
Received 8 September 2015
Revised 9 February 2016
Accepted 11 February 2016
Available online 27 February 2016

Keywords:
Reinforced Concrete (RC)
Structural Health Monitoring (SHM)
Beam
Shear
Piezoelectric lead Zirconate Titanate (PZT)
PZT sensor/actuator
Electro-Mechanical Impedance (EMI)
Electro-Mechanical Admittance (EMA)
Damage assessment
Experimental testing

ABSTRACT

The ability of a new portable real-time Wireless impedance/Admittance Monitoring System (WiAMS) in damage diagnosis of shear-critical RC beams is experimentally studied. This system is based on the electromechanical impedance concept integrating piezoelectric transducers in reinforced concrete structural elements. The proposed monitoring method uses WiAMS devices and an array of embedded "smart aggregates" and externally bonded piezoelectric transducers. Five shear-critical beams are tested in order to evaluate the ability of the proposed methodology in damage detection and assessment. Voltage signatures of the piezoelectric transducers have been measured at the healthy state and at different damage levels of the beams. Quantitative assessment of the damage using values of statistical damage index is also presented and discussed. Test results showed that transducers close to the diagonal cracking provided sound and gradual differences between the signatures at the healthy state and each damage level. Voltage responses and index values of the transducers located on the shear span where the critical crack formed provided cogent evidence of damage and their gradual character revealed the magnitude of damage. Promising results concerning the prediction of the forthcoming final shear failure at earlier damage stages such the onset of diagonal cracking have also been derived.

1. Introduction

Recent development of various experimental approaches that prevent catastrophic failures and reduce cost of inspection in Reinforced Concrete (RC) infrastructures has been emerged from the necessity of real-time damage detection and Structural Health Monitoring (SHM) techniques. SHM aims to develop efficient methods for the continuous inspection and detection of various defects in civil engineering structural members. Even more, SHM is becoming extremely important in RC structures that are governed by shear mechanisms which lead to fragile and abrupt failure modes. Even minor incipient shear damage to deficient shear-critical RC elements, such as beam–column joints, short columns and deep beams, could be the cause of catastrophic collapse. Many collapse accidents in RC structures have been reported over the past two decades that were initiated from local failure of the shear-critical members [1–5].

Nowadays, the development of SHM techniques is very rapid, especially of those based on the implementation of smart materials such as Piezoelectric lead Zirconate Titanate (PZT). The Electro-Mechanical Impedance (EMI) or its reverse Electro-Mechanical Admittance (EMA) technique is one of the SHM techniques based on piezoelectric materials, which is a powerful health monitoring technique for civil structure systems [6–9].

A PZT transducer produces electrical charges when subjected to a strain field and conversely it produces mechanical strain when an electrical field is applied. A theoretical model of the PZT functioning has been proposed by Liang et al. [10]. The SHM and damage detection techniques have been developed based on the coupling properties of the piezoelectric materials. The impedance-based SHM approach utilizes the EMI of these materials that is directly related with the mechanical impedance of the host structural members, a property that is directly affected by the presence of any structural damage. Thus the impedance extracts and its inverse, the admittance, constitute the properties on which the PZT approach is based for the SHM of RC structures. Specifically, the produced effects by the structural damages on the PZT electrical signatures are vertical enlargement or/and lateral shifting of the baseline signatures of the initially healthy structure. These effects are the main damage indicators for damage detection and evaluation that many researches are based on [4,11].

* Corresponding author.
E-mail addresses: mvoutetaki@isc.tuc.gr, mvoutetaki@yahoo.com (M.E. Voutetaki).

http://dx.doi.org/10.1016/j.engstruct.2016.02.014
0141-0296/

Divsholi and Yang [12] used PZT transducers for the detection of damage location and severity level and Yang et al. [13] used the structural mechanical impedance extracted from the PZT signature as the damage indicator for the detection of structural damages in a 2-story RC frame. Further, PZT transducers bonded on steel reinforcing bars that were embedded in concrete specimens were also applied in order to perform non-destructive monitoring of the bond development between bar and concrete [11,14].

Providakis and Voutetaki [15] presented a numerical method for structural health monitoring and damage identification of a concrete beam by extracting the electromechanical impedance characteristics of surface bounded self-sensing PZT patches. The damage was firstly quantified conventionally by the root mean square deviation index and then by using a statistical confidence method in system identification advanced routines of a mathematical computational software. Numerical studies that simulate EMA monitoring procedures utilizing PZTs to detect and localize cracking in concrete beams have also been presented [16–20]. Further, identification of damages due to the corrosion of steel reinforcing bars and debonding between bars and concrete have been investigated experimentally and analytically using bonded PZT transducers [11,21,22]. Furthermore, real-time monitoring of concrete compressive strength gain using bonded PZT patches showed promising results [23–27].

Two different installations of PZT transducers have been used to monitor concrete structural elements and specimens; embedded PZTs inside concrete mass as "smart aggregate" and external piezoelectric patches bonded on the surface of concrete. It has been found so far that the surface bonded PZTs are not effective for monitoring a large area or the entire concrete structure due to their small sensing range. On the other hand, the embedded PZT transducers as smart aggregates using the wave transmission technique that is based on electrical wave transmission can be employed to monitor large areas with a reasonably low actuation signal [28–32].

It is noted that most of the developed SHM systems using EMI technique and PZT transducers, so far, are not portable and therefore they have obvious difficulties and limitations to be in-situ applied in existing structures. There are only a few portable and wireless EMI monitoring systems using PZTs for concrete structures that recently have been developed [5,25,26,33–37]. The innovative, wireless, portable, lightweight, real-time impedance monitoring sensing system that is experimentally investigated herein has initially been used to monitor early-age concrete compressive strength gain [25,26,36] and flexural RC members under cyclic deformations [38].

Failures in shear-critical RC elements are associated with brittle collapses, usually without reaction capacity by users that might lead to human and material losses. When principal tensile stresses exceed the tensile strength of concrete, diagonal cracking occur in the shear span and the behaviour of a concrete element under shear stresses is mainly characterised by the tensile strength of the material [39–43]. It has also been found that the ratio of the transverse shear reinforcement, the ratio of the tensional reinforcement and the span-to-depth ratio control the inclination of the shear diagonal cracking of shear-critical RC beams [44]. It is also known that the ultimate shear strength of RC beams is calculated by a superposition of the shear strength of beams without web reinforcement and the strength provided by the shear reinforcement [45,46]. However, the formation of the critical shear diagonal cracking of RC beams without web reinforcement is crucial for the determination of the onset of diagonal cracking of common RC beams with bars and stirrups. Consequently, any improvement of the existing SHM techniques to detect in real-time the first appeared diagonal cracks in a RC beam and to assess their severity before inevitable brittle shear failure of the element is essential [47].

In this work the developed Wireless impedance/Admittance Monitoring System (WiAMS) is experimentally investigated in shear-critical RC beams. This new wireless, portable, lightweight, real-time impedance monitoring system is applied to five large-scale RC beams failing in shear in order to evaluate its ability in damage detection and assessment. Voltage signatures of an array of embedded piezoelectric transducers as "smart aggregates" and externally bonded piezoelectric patches have been measured at different levels of applied load and corresponding damage states. Quantitative assessment of the examined damage levels using values of statistical damage index is also attempted. The basic concept of this study is to address a new monitoring experimental method using WiAMS in shear-critical RC elements in order to diagnose damage and predict the forthcoming total shear failure at early damage stages, such as at the onset of diagonal cracking.

2. Damage evaluation procedure using Electro-Mechanical Impedance (EMI) or its inverse Electro-Mechanical Admittance (EMA)

The Electro-Mechanical Impedance technique uses Piezoelectric lead Zirconate Titanate transducers exhibiting their characteristic feature to generate surface electric charge in response to an applied mechanical stress and undergo mechanical deformation in response to an applied electric field. Thus, when a mounted PZT on a structure is actuated, a potential damage induces change in the mechanical impedance (or its reverse admittance) of the structure and this change reflects on the electrical signature of the PZT. When a structure is regularly monitored by extracting the signal to the exciting frequency of the installed PZTs, the changes in their signatures become indicative of the presence of structural damage [16,18,48]. This way, any concrete cracking or steel yielding (structural damages) can be detected using the changes of the signatures of the mounted piezoelectric transducers.

In the adopted structural health monitoring methodology for the detection of a potential damage in RC beams the PZT transducers are excited for a specific frequency range and their corresponding signals are recorded simultaneously. These measurements are carried out initially on the undamaged RC beam (initial status) in order to record the healthy condition and to be used as a reference signature. Afterwards, the same measurements are carried out on the damaged RC beam at different levels of damage. More details about the overall concept of the adopted EMI technique could be found in the works of Providakis et al. [11,18,19,22].

Selection of the excitation frequencies of the mounted PZTs is an important parameter affecting the effectiveness of the method and therefore special attention has been given [22]. It has been proven that damage detection capability greatly depends on the successful frequency selection of the excitation rather than on the voltage of the excitation loading itself [20]. This observation demonstrates that excitation loading sequence can have a voltage level low enough that the technique may be considered as easily applicable and effective for real structures. In this study analyses are performed for a frequency range of 10–260 kHz per step of 10 kHz by using one cycle per 10 kHz. A harmonic excitation voltage of 10 V is amplified to the PZT transducers in time domain range at every central frequency, as described by the expression:

$$V_{PZT}(t) = 10\sin(2\pi\omega t) \quad (1)$$

where V_{PZT} is the excitation voltage of the PZT, ω is the angular frequency of the driving voltage and t is the time domain range.

The interaction between PZT and the RC element is captured in the form of an admittance signature consisting of the conductance (real part) and the susceptance (imaginary part). As a result of these interactions, structural characteristics are reflected in the signature. The one-dimensional vibrations of the PZT patch are governed by the differential equation derived by Liang et al. [10] based on dynamic equilibrium of the PZT transducer. Bhalla and Soh [49] extended this approach to two dimensional structures by introducing the concept of effective impedance, deriving following expression for complex admittance of the mounted PZT patch:

$$\overline{Y} = \frac{\overline{I}}{\overline{V}} = G + Bj = 4\omega j \frac{L^2}{h}\left[\bar{\varepsilon}_{33}^{T} - \frac{2d_{31}^2 \overline{Y}^{E}}{(1-\nu)} + \frac{2d_{31}^2 \overline{Y}^{E}}{(1-\nu)}\left(\frac{Z_{a,eff}}{Z_{s,eff}+Z_{a,eff}}\right)\left(\frac{\tan(kL)}{kL}\right)\right] \quad (2)$$

where $\overline{V}$ is the harmonic alternating voltage supplied to the circuit, $\overline{I}$ is the current passing through PZT, G is the conductance (the real part of admittance), B is the susceptance (the imaginary part of admittance), j is the imaginary unit, ω is the angular frequency, L is the half-length of the patch, h is the thickness of the patch, d_{31} is the piezoelectric strain coefficient of the PZT, $Z_{a,eff}$ is the short-circuited effective mechanical impedance, $Z_{s,eff}$ is the effective structural impedance, ν is Poisson's ratio, k is the wave number related to the angular frequency, $\overline{Y}^{E}$ is the complex Young's modulus of elasticity under constant electric field and $\bar{\varepsilon}_{33}^{T}$ is the complex electric permittivity of PZT patch along axis "3" at constant stress. Any damage to the concrete element that changes its mass and stiffness characteristics will cause the structural parameters to change and will thus alter the effective structural impedance, which in turn changes the admittance in previous equation, thus serving as an indicator of the state of health of the element [21].

The absolute value of the admittance is calculated by the following equation:

$$|Y(\omega)| = \sqrt{G^2(\omega) + B^2(\omega)} \quad (3)$$

3. The developed wireless structural health monitoring system (WiAMS)

The overall test setup and the wireless monitoring system of the developed SHM methodology for the in-situ detection of damages in real-scale reinforced concrete beams is shown in Fig. 1. It is a specially implemented wireless monitoring system that is based on the Electro-Mechanical Impedance methodology or its inverse Electro-Mechanical Admittance and utilizes the measurements of Piezoelectric lead Zirconate Titanate transducers mounted to the structural element which operate as actuators and sensors simultaneously.

WiAMS is a Wireless impedance/Admittance Monitoring System that estimates the impedance magnitude of a piezoelectric transducer that is utilized in order to monitor in situ and in real-time the structural integrity of concrete members and structures. This way, a WiAMS device sends out the interrogating waves through a PZT and receives the reflected waves at the same time. It offers extensive features such as remote control, high processing power, wireless data upload to SQL database, email notifications, scheduled, iterative impedance magnitude estimations and frequency span from 5 kHz to 300 kHz with 1 Hz resolution. The WiAMS device is consisted of the following multiple custom-made modules [37,38,50], as it is also shown in Fig. 2:

1. A single board computer (SBC) Raspberry Pi.
2. A custom board with the AD7357 ADC.
3. A custom board with the AD9837 frequency generator.
4. A custom interface board responsible for the power supply and the connection of the rest modules between them and with the Raspberry Pi.
5. The PZT driver module.

The impedance magnitude of the PZT is estimated by WiAMS based on the following consideration. First, the input sinusoidal voltage signal can be expressed as a function of time in the form:

$$V_{PZT}(t) = V_p \sin(\omega t) \quad (4)$$

where $V_{PZT}(t)$ is the voltage across the direction of the axis of the width of the PZT at time t, V_p is the peak voltage of the voltage signal and ω is the radial frequency. The relationship between the radial frequency ω (in radians/s) and the frequency f (Hz) is $\omega = 2\pi f$.

In a linear system the response current signal $I(t)$ is shifted in phase φ and has a different peak current I_p:

$$I(t) = I_p \sin(\omega t + \varphi) \quad (5)$$

Taking into account that every PZT transducer under a pure and high frequency sinusoidal voltage signal behaves almost like a capacitive system that tends to preserve negligible phase difference between voltage and current output signal, the impedance magnitude of the PZT at radial frequency $|Z(\omega)|$ can be evaluated by the expression:

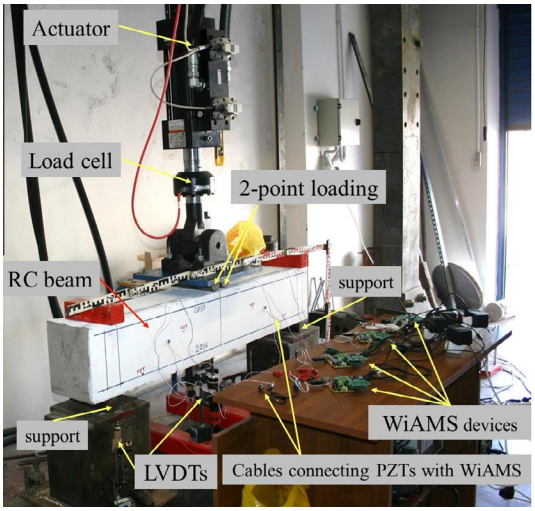

Fig. 1. Test setup and wireless monitoring system of large-scale RC beams.

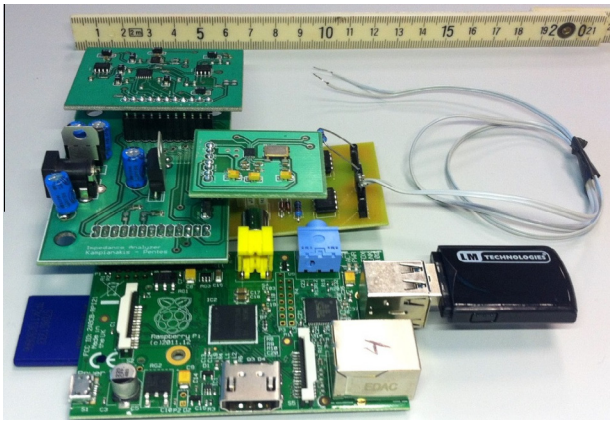

Fig. 2. The Wireless impedance/Admittance Monitoring System (WiAMS) device for the in-situ structural health monitoring of reinforced concrete members and structures.

$$|Z(\omega)| = \frac{1}{|Y(\omega)|} = \frac{V_p(\omega)}{I_p(\omega)} \cong \frac{V_p(\omega)}{\frac{V_{in}(\omega)}{|Z(\omega)|+R_f}} \quad (6)$$

where V_{in} is the voltage output of the frequency generator and R_f is a resistor connected in series with the PZT of a circuit that consists an efficient and simple method to measure impedance magnitude by exciting the device under test with a sinusoidal signal and measuring the amplitude of the voltage of the device [37,38,50].

Solving Eq. (6) in terms of $V_p(\omega)$ the peak value of the voltage across the PZT transducer can be estimated by:

$$V_p(\omega) \cong \frac{|Z(\omega)|}{|Z(\omega)| + R_f} V_{in}(\omega) \quad (7)$$

Based on the above equation, it is obvious that the voltage across the PZT transducer and especially the peak voltage signal $V_p(\omega)$ provides a solid indication for the value of $|Z(\omega)|$ being directly dependent on any observed impedance amplitude variations. This way, under steady state conditions, if structural integrity condition of the host structure changes the peak amplitude of the voltage signal across the PZT transducer also changes. The application of the expression (7) enables the implementation of simple and low-cost monitoring topologies compared to the traditional and complex impedance analysers. Further details concerning the hardware elements, the modules functionality of WiAMS, its calculating capabilities and its ability to be applied in concrete cubes and prisms could be found in the recent work of Providakis et al. [50].

In order to investigate the design of the experimental setup using the developed monitoring procedure a group of shear-critical RC beams were subjected to a typical two-point loading till failure. During testing, the voltage signals of embedded and surface bonded piezoelectric transducers have been measured at different loading – damage levels. Each voltage versus frequency signature curve corresponds to an average of three repeated measurements. These curves have also been used for the quantitative assessment of the imposed damage levels using the values of a statistical index.

4. Experimental investigation and implementation of WiAMS for damage evaluation in shear-critical RC beams

4.1. Installation of PZT transducers

PZT transducers with dimensions 10 mm × 10 mm and material mark designation PIC 255 are used. PZTs have been mounted to the tested RC beam as (a) embedded PZTs inside the concrete mass of the beams as "smart aggregates" and (b) externally epoxy bonded PZT patches at the surface of the beams.

Characteristics (geometrical, reinforcement and PZT transducers) of a typical tested shear-critical RC beam with embedded "smart aggregates" and externally epoxy bonded PZTs are displayed in Fig. 3. The preparation of the embedded PZT transducers as "smart aggregates" includes the following steps: Two cables are soldered to each side of the PZT; epoxy adhesive is used to coat and to waterproof the patches; cement paste is poured in small foam moulds enclosing the waterproofed PZT patches. In a few days and after demoulding the hardened cement paste, irregular cement cubes with the enclosed PZTs were formed as "smart aggregates". The PZT "smart aggregates" have been fixed inside the wooden mould of the RC beams, after the placement of the steel reinforcing bars and stirrups, just before concrete casting. Embedded "smart aggregates" have been installed at each shear span and their positions were close to the potential future diagonal cracks (see also Fig. 3).

The procedure adopted for the protection of the fragile piezoelectric transducers and their installation inside the concrete beam as "smart aggregates" was based on the work of Song et al. [28]. The waterproof epoxy adhesive was first used as an insulation coating of the transducer to prevent water and moisture damage. The integrity of each transducer has been checked by admittance measurements before and after embedded into a small concrete block to form a "smart aggregate". The "smart aggregate" has been embedded at the desired position inside the beam before concrete casting, eliminating the risk of damaging the transducer during the vibrating process [28].

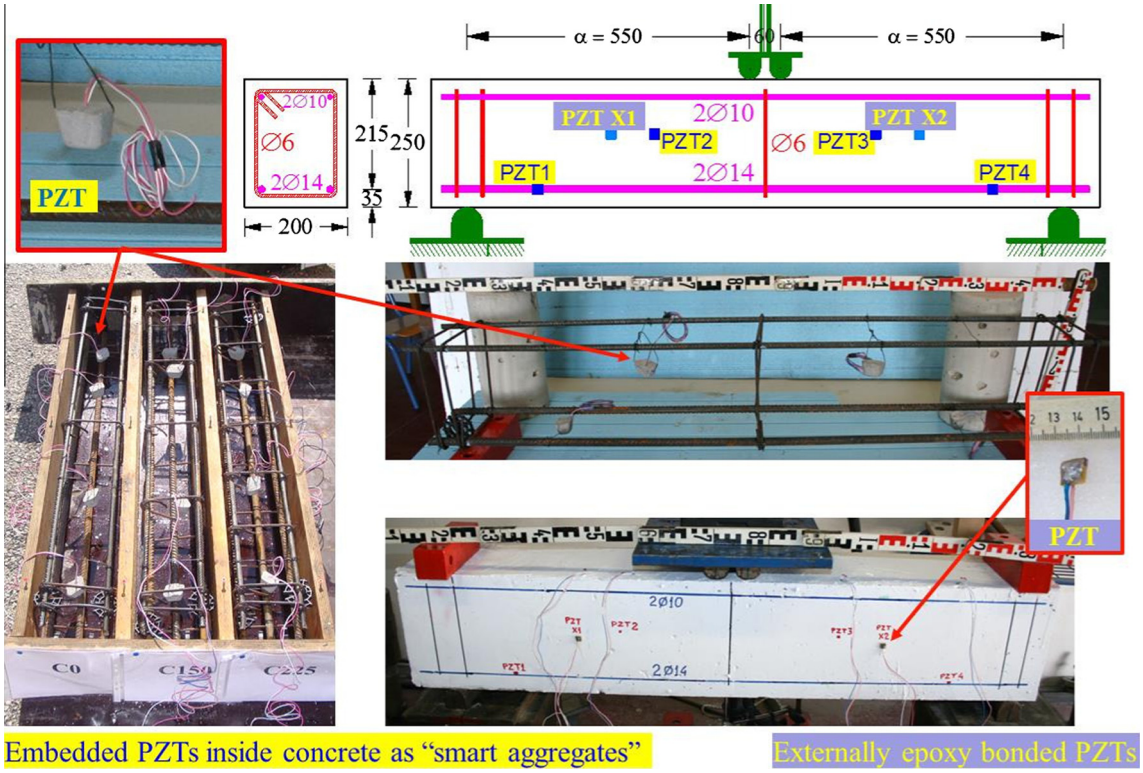

Fig. 3. Typical characteristics (geometrical, reinforcement and PZT transducers) of a tested shear-critical reinforced concrete beam.

After concrete casting and demoulding the hardened concrete of the beams, PZT transducers with two soldered cables were carefully epoxy bonded on the concrete surface of the RC beams at each shear span, close to the potential future diagonal cracks (see also Fig. 3). Epoxy adhesive of high shear modulus and very small thickness approximately to one-third of the thickness of the PZT transducer has been used to bond each PZT to the concrete surface [51].

The combined implementation of embedded smart piezoelectric aggregates and externally epoxy bonded piezoelectric patches has recently been applied to detect damage in concrete beams [30,52]. First test results showed that "smart aggregates" can detect the discontinuities and monitor large areas whereas surface bonded piezoelectric patches using wave propagation technique are sensitive to localized damage. Unlike steel structures for which large area can be monitored using the EMI technique, in concrete structures the EMI sensing region is small due to the high damping of the concrete. Thus, Divsholi and Yang [30] suggested that the combination of embedded PZTs using the wave transmission technique to monitor the overall condition of the element and surface bonded PZTs using the wave propagation technique to monitor the important sections of structure can be an effective SHM method. This combined concept has been extended herein by the use of a new wireless monitoring system in shear-critical concrete beams in order to diagnose cracking and to predict the forthcoming diagonal failure at early damage stages.

4.2. RC beam characteristics, test setup and instrumentation

The test program includes the application of the developed wireless monitoring platform (WiAMS) to five shear-critical RC beams. The effectiveness of WiAMS to evaluate the damages (cracks) caused on the RC beams during a typical two-point loading test and at different levels of loading and corresponding damage is experimentally investigated. The geometrical and reinforcement characteristics of the tested RC beams are shown in Fig. 4a and b. Beams are sorted to two different groups; group A and group C that consists of two and three beams, respectively. The mean concrete cylinder compressive strength of the beams equals to 29.1 MPa.

The total length of group A beams is 1.30 m, the shear span is a = 0.55 m, the width to the height ratio is b/h = 200/250, the effective depth is d = 215 mm and the span-to-depth ratio is a/d = 2.56. The bottom tensional longitudinal reinforcement of the beams comprises two steel bars of diameter 14 mm (2∅14) and the top compression reinforcement is two bars of diameter 10 mm (2∅10). Both shear spans of the first beam (beam A0) have no transverse web reinforcement in order to control a typical shear failure of a beam without stirrups (design of a typical shear-critical RC beam) and only a few closed stirrups of diameter 6 mm have been used just to hold longitudinal reinforcing bars in place. In order to examine thoroughly only the critical shear span of the beam in which final shear diagonal failure inevitable will occur (left shear span), the second beam of group A (beam A0a) has transverse web reinforcement (closed steel stirrups ∅6/110 mm) only in the right shear span.

The total length of group C beams is 1.10 m, the shear span is a = 0.45 m, the width to the height ratio is b/h = 150/150, the effective depth is d = 125 mm and the span-to-depth ratio is a/d = 3.6. The bottom tensional longitudinal reinforcement of the beams comprises three steel bars of diameter 14 mm (3∅14) and the top compression reinforcement is two bars of diameter 10 mm (2∅10). Both shear spans of the first beam (beam C0) have no transverse web reinforcement in order to control a typical shear failure of a beam without stirrups and only a few closed stirrups of diameter 6 mm have been used just to hold longitudinal reinforcing bars in place. Further, in order to investigate the effectiveness of the proposed structural monitoring technique in common shear-critical RC beams with web reinforcement, beams C150 and C225 have closed steel stirrups of diameter 6 mm spacing per 150 mm (∅6/150 mm) and per 225 mm (∅6/225 mm), respectively.

Nineteen PZT transducers were embedded inside the concrete mass of the RC beams as "smart aggregates" (PZT1 to PZT19) and eleven PZT patches were epoxy bonded externally on the concrete surface of the RC beams (PZTX1, PZTX2, PZTX5, PZTX6, PZTX7, PZTX9, PZTX10, PZTX13, PZTX14, PZTX17 and PZTX18). The exact locations of all PZTs ("smart aggregate" transducers and externally bonded patches) mounted to each beam are displayed in Fig. 4 and summarized in Table 1.

Test setup and instrumentation of the shear-critical RC beams is also shown in Fig. 1. Tested beams were simply supported on a rigid laboratory frame using two roller supports at a distance of 1.16 m and 0.96 m for the beams of group A and C, respectively. The imposed loading was applied at two points 60 mm apart from each other in the mid-span of each beam using a steel spreader beam. The imposed load was consistently increased with low rate using a pinned-end actuator and was measured by a load cell with accuracy equal to 0.05 kN. The net mid-span deflections of the tested beams were recorded by three Linear Variable Differential Transducers (LVDTs) with 0.01 mm accuracy. One of them was placed at the middle of the beam span and the other two at the supports (Fig. 1). Measurements for load and deflection were read and recorded continuously during the tests. Further, admittance measurements of the embedded piezoelectric transducers inside concrete mass as "smart aggregates" and the externally epoxy bonded PZTs were recorded at different levels of the applied loading using the WiAMS experimental setup shown in Fig. 1. A harmonic excitation voltage of 10 V is amplified to the mounted PZTs in time domain range at every central frequency, as described by the expression (1). It is noted that each WiAMS device records the measurements of only one piezoelectric transducer. Since six transducers (embedded and surface bonded) have been installed in each tested beam, six WiAMS devices were needed and used for the measurement of all six transducers simultaneously. Nevertheless, if the monitoring procedure requires more transducers than the available devices, the loading and therefore the corresponding damage should be kept constant during the measurements of each transducer.

4.3. Test results and discussion

Tested RC beams exhibited typical shear response and brittle diagonal failure, as they have been designed and expected. In general first flexural cracks formed in the mid-span and perpendicular to the longitudinal axis of the beams. The increase of the applied load caused further flexural cracks that spread and inevitably initial diagonal cracks formed. Consequently, the formation of a critical shear crack on a shear span of each beam caused its brittle failure. The plots of Figs. 5–9 present the behaviour of each beam in terms of experimental curve of shear load versus mid-span deflection. Further, the cracking patterns of the RC beams at different levels of loading and corresponding damage are also displayed in the photographs of Figs. 5–9. The positions and the names of the PZTs are also mentioned in the same figures for comparison reasons.

Further, Table 2 presents the value of the applied load (shear force) in terms of ultimate shear strength percentage at each examined loading level in which PZT voltage signals have been measured using WiAMS for each beam. A brief description of the corresponding damage at each loading level is also summarized in Table 2. Voltage signals of the mounted PZT transducers were measured at the beginning of the test ("Healthy state") and at the damaged levels shown in Table 2. This way, the examined

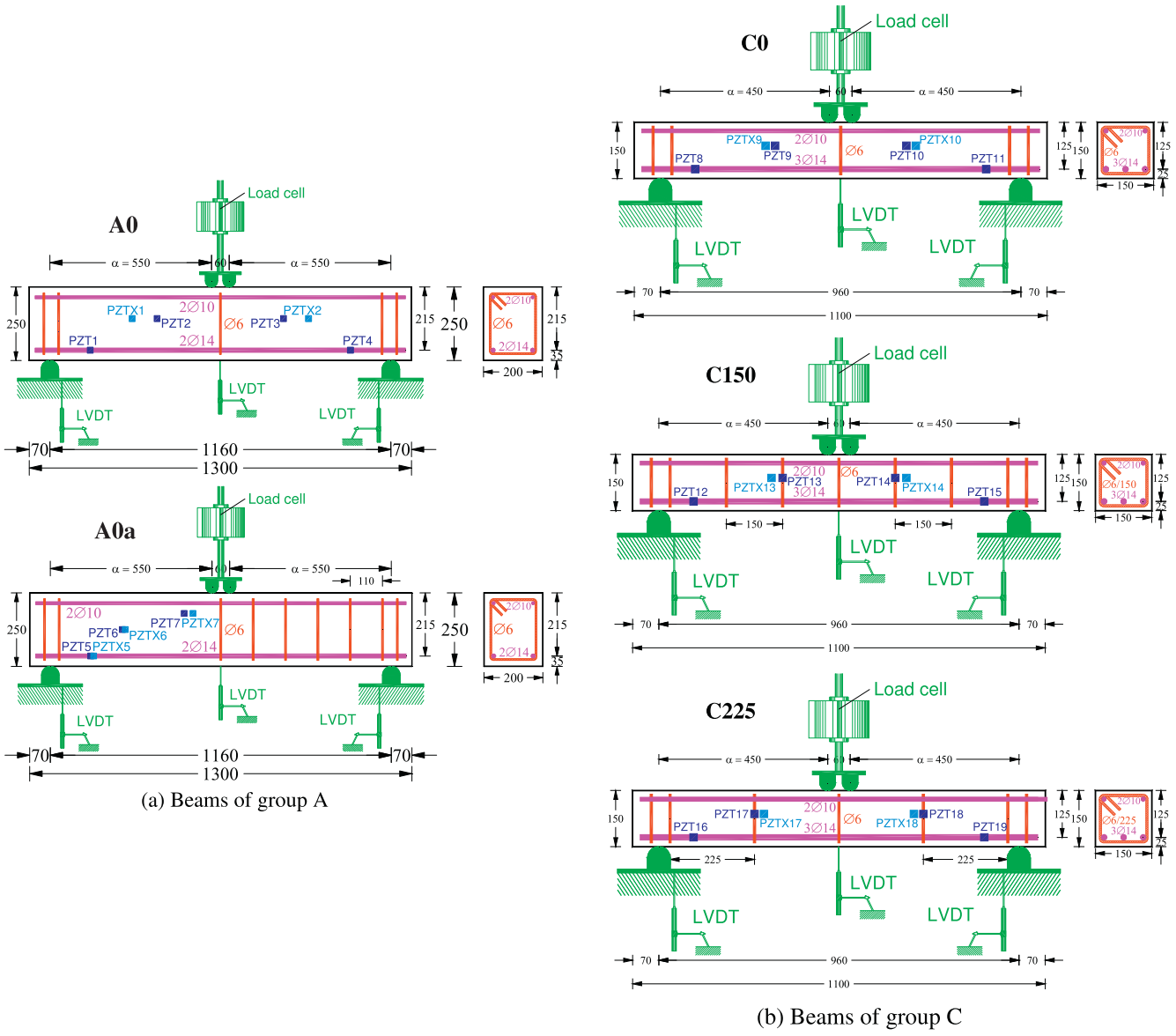

(a) Beams of group A

(b) Beams of group C

Fig. 4. Geometrical and reinforcement characteristics of the tested beams.

Table 1
Positions of the mounted PZTs on the shear spans of the tested RC beams.

Beam code name	Smart aggregates PZT transducers		Externally bonded PZT patches	
	Left shear span	Right shear span	Left shear span	Right shear span
A0	PZT1, PZT2	PZT3, PZT4	PZTX1	PZTX2
A0a	PZT5, PZT6, PZT7	–	PZTX5, PZTX6, PZTX7	–
C0	PZT8, PZT9	PZT10, PZT11	PZTX9	PZTX10
C150	PZT12, PZT13	PZT14, PZT15	PZTX13	PZTX14
C225	PZT16, PZT17	PZT18, PZT19	PZTX17	PZTX18

loading level corresponds to a specific damage level that also displayed in the cracking patterns of the beams in Figs. 5–9.

Concerning the WiAMS measurements of the mounted PZTs, Figs. 10 and 11 display the voltage signals of the embedded in the left shear span of beam A0 "smart aggregate" transducers PZT1 and PZT2, respectively, versus the frequency range of 10–260 kHz. In the same way and for the same frequency range (10–260 kHz) the diagram of Fig. 12 demonstrates the experimentally measured voltage signals of the externally epoxy bonded PZTX1 on the left shear span of beam A0. A close-up of this curve is also displayed in Fig. 12 in order to discern the differences of the PZTX1 signals between the healthy and the examined damage states.

Typical curves of voltage signal measurements of embedded "smart aggregate" transducers are also presented in Figs. 13 and 14 for PZT9 of beam C0 and PZT18 of beam C250, respectively.

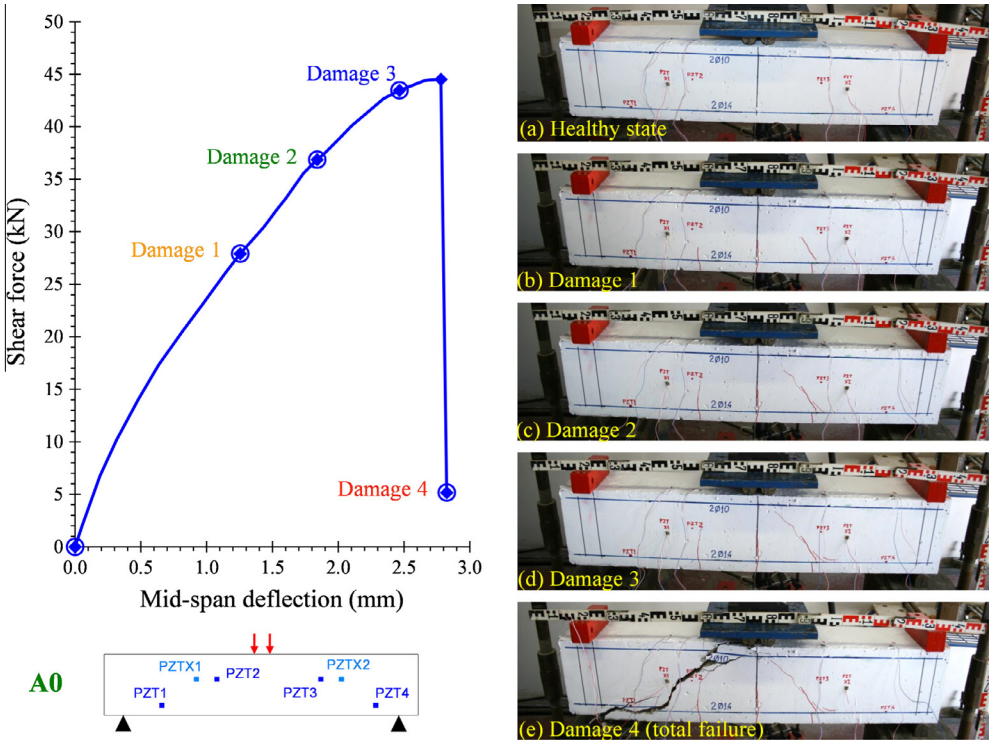

Fig. 5. Experimental response and cracking patterns at different damage – loading levels of the beam A0.

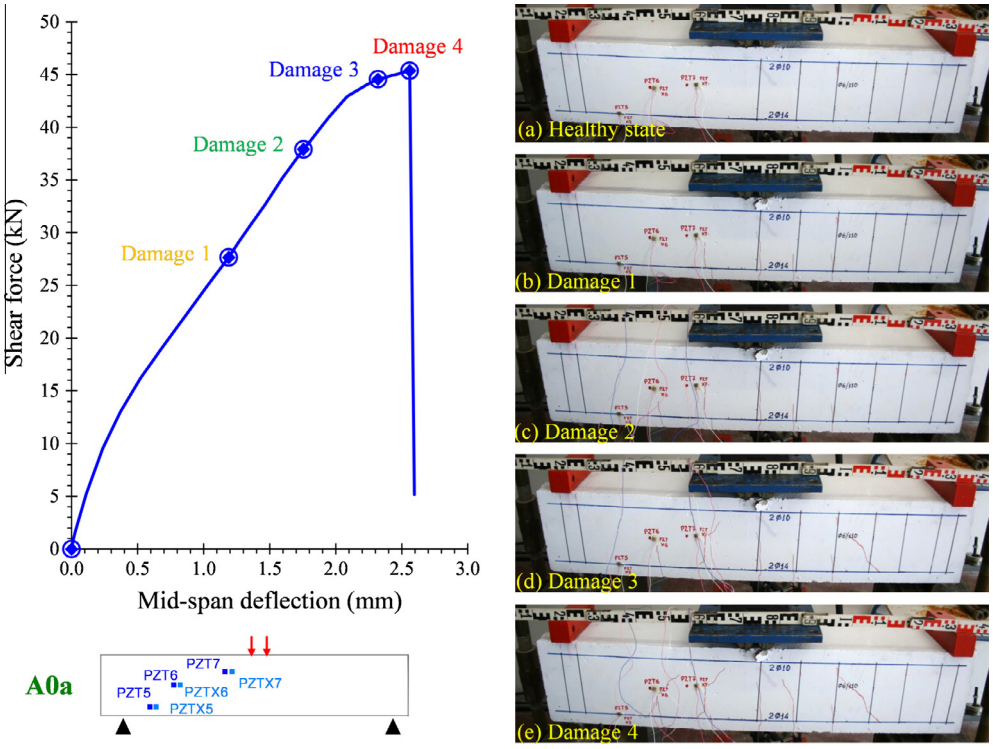

Fig. 6. Experimental response and cracking patterns at different damage – loading levels of the beam A0a.

Further, typical voltage signal versus frequency curves of the externally epoxy bonded patches PZTX6 and PZTX7 (placed on the left shear span of beam A0a) are displayed in Figs. 15 and 16, respectively. Furthermore, Figs. 17 and 18 demonstrate the voltage signal measurements of the externally bonded PZTX13 on the left and of the externally bonded PZTX14 on the right span of beam C150, respectively.

The comparisons of the curves in Figs. 10 and 11 clearly show that there are certain discrepancies between the healthy and the damaged levels that have been measured from the embedded

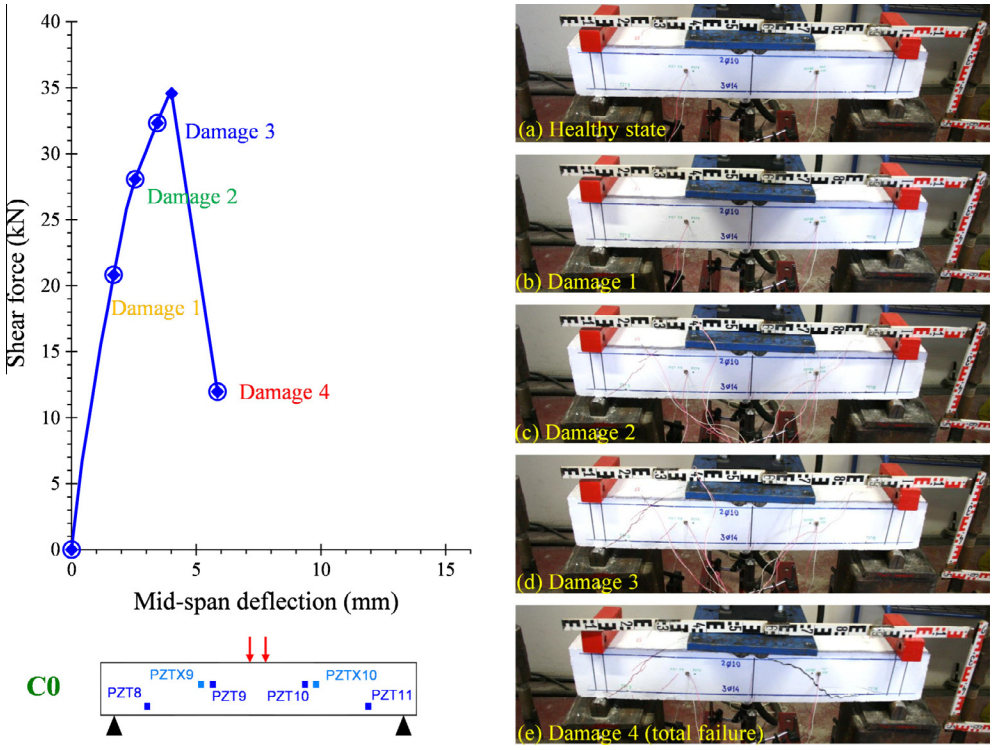

Fig. 7. Experimental response and cracking patterns at different damage – loading levels of the beam C0.

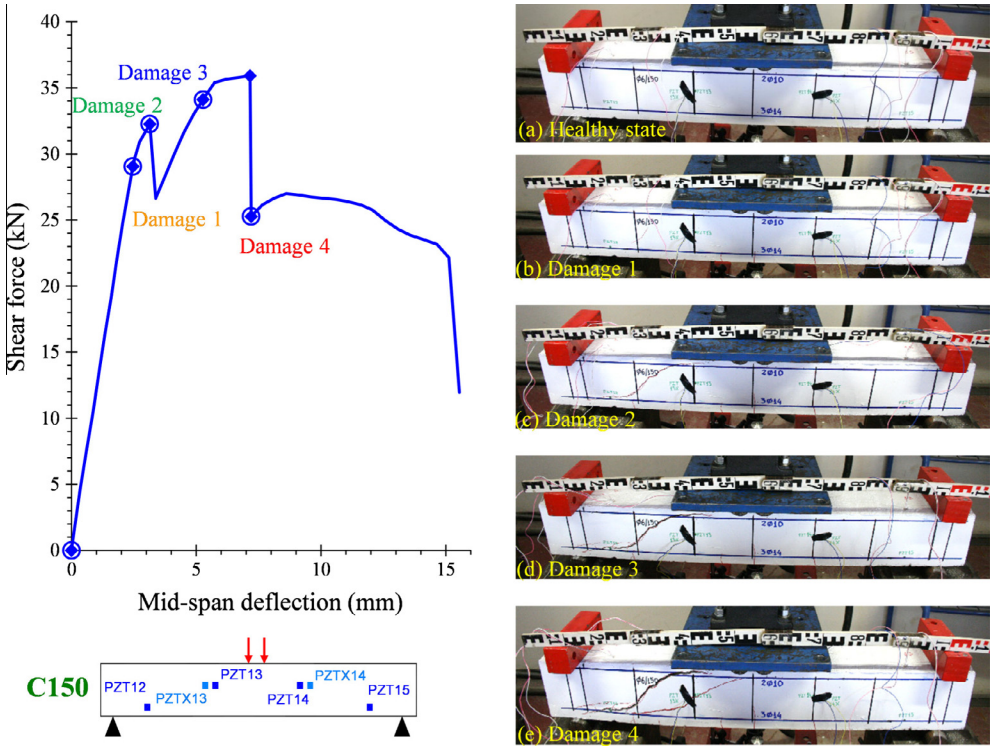

Fig. 8. Experimental response and cracking patterns at different damage – loading levels of the beam C150.

"smart aggregate" transducers PZT1 and PZT2, respectively. Especially, PZT2 voltage signal curves display higher discrepancies between the "Healthy" state and the "Damage 3" level than these between "Healthy" and "Damage 2" and also between "Healthy" and "Damage 1". In these Figures the corresponding discrepancies measured from PZT1 are less than those of PZT2. This fact indicates that "smart aggregate" transducer PZT2 seems to be more sensitive to the identification of the examined damage levels than the "smart aggregate" transducer PZT1. This is associated to the distance between these two "smart aggregate" transducers and the occurred flexural cracks of "Damage 1" and the developed cracking in "Damage 2" and "Damage 3" level; PZT2 is located closer to the

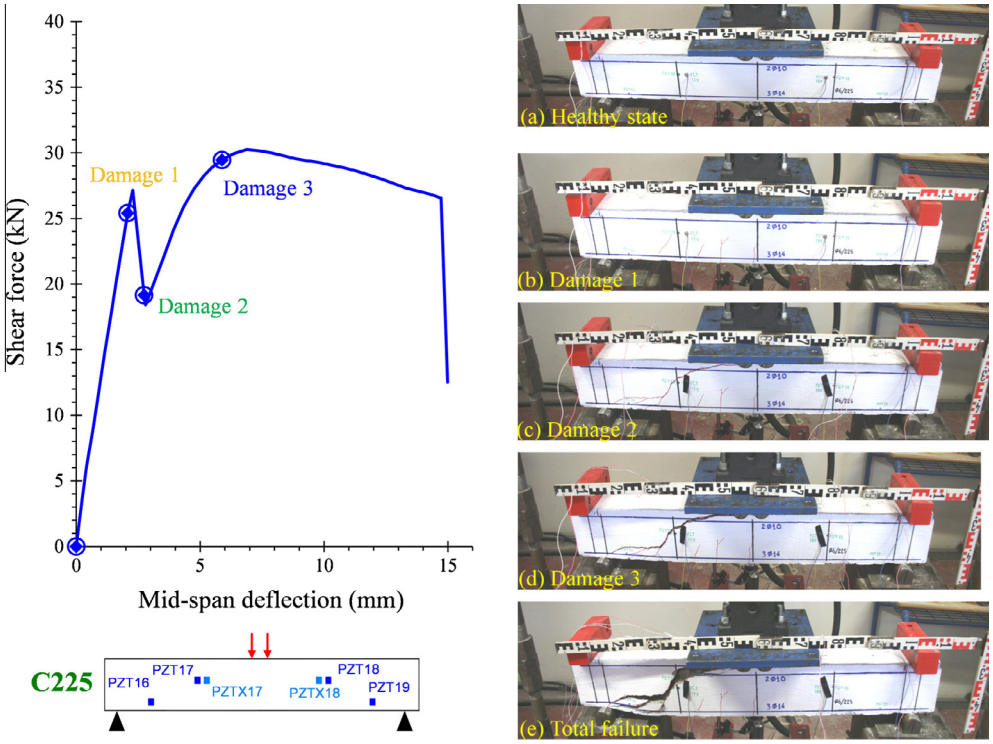

Fig. 9. Experimental response and cracking patterns at different damage – loading levels of the beam C225.

cracks developed at damage levels 1, 2 and 3 than PZT1 (see also Fig. 5). Therefore, PZT2 transducer greatly senses the material anomaly caused by the cracking and provides sound and gradual voltage signal measurements for the examined damage levels.

It is also noted that the discrepancies between the healthy and the damaged levels in the voltage signal curves of the embedded "smart aggregate" transducers PZT1, PZT2, PZT9 and PZT18 (Figs. 10, 11, 13 and 14, respectively) are clear and higher than the corresponding discrepancies for the voltage signals of the externally bonded piezoelectric patches PZTX1, PZTX6, PZTX7 and PZTX13 (Figs. 12, 15, 16 and 17, respectively) which seem to be rather slight. This indicates that the externally bonded and the embedded transducers seem to have different sensitivity since the surface bonded ones are sensitive to surface local damage whereas the "smart piezoelectric aggregates" are sensitive to inside local damage. Also, it should be mentioned that all the externally bonded PZT patches succeeded to measure voltage signals in all the examined damage levels (all 4 levels), whereas many embedded "smart aggregate" transducers (such as PZT1 and PZT2) failed to measure the voltage signals in the last damage level (Damage 4 – total failure). This is justified to the formation of the critical wide diagonal crack that occurred during the final shear failure of the beams and interrupted the operation of the embedded "smart aggregates".

From the comparison of the voltage signal curves between "smart aggregate" transducers PZT9 and PZT18 in Figs. 13 and 14, respectively, it is obvious that PZT9 exhibits greater discrepancies between the healthy state and the examined damaged levels with respect to the corresponding discrepancies of PZT18 which are slight and rather negligible for the damage levels 1, 2 and 3. This observation is corresponding to the fact that PZT18 is placed on the right shear span of beam C225 where no diagonal cracking occurred (critical shear crack formed on the left span, as shown in Fig. 9).

Further, the comparison of the voltage signal curves between externally bonded patches PZTX13 and PZTX14 in Figs. 17 and 18, respectively, reveal that PZTX13 displayed greater discrepancies between the healthy state and the examined damaged levels with respect to the corresponding discrepancies of PZTX14 which are negligible. This is justified by the fact that PZTX13 is placed on the left shear span of beam C150 where severe diagonal cracking occurred and critical shear crack formed (see also Fig. 8). Thus, since the right shear span remained more or less undamaged (see also Fig. 8) the unchangeable voltage signal measurements of PZTX14 in curves of Fig. 18 seem positively rational confirming the damage occurred at the other (left) shear span.

It is mentioned that temperature and humidity effects are not considered in this study, while temperature and humidity conditions remained constant during the test procedure. However, it should be kept in mind that temperature and humidity variation results in significant variation in the impedance measurement that may lead to erroneous diagnostic results regarding the integrity of real structures [53].

4.4. Quantification of damage

The previously presented and discussed voltage signal response plots provide a qualitative approach for damage detection and identification of the tested shear-critical RC beams. The quantitative assessment of damage is traditionally made by the use of the statistically scalar damage values of Root Mean Square Deviation index (RMSD) [54,55]:

$$\mathrm{RMSD} = \sqrt{\frac{\sum_1^N \left(|V_p(\omega)|_D - |V_p(\omega)|_0\right)^2}{\sum_1^N \left(|V_p(\omega)|_0\right)^2}} \tag{8}$$

where $|V_p(\omega)|_0$, $|V_p(\omega)|_D$ are the absolute values of the voltage signal measurements of the examined piezoelectric transducer at the baseline value (subscript 0) of the initial RC beam status ("Healthy" state) and at the examined damage level (subscript D) of the RC beam ("Damage 1", "Damage 2", etc.), respectively, and N is the

Table 2
Damage identification and description based on the level of the applied load and the shear strength of each tested RC beam.

Beam code name	Damage	Shear load (percentage of the ultimate shear capacity V_u)	Damage brief description
A0	Damage 1	60%	Flexural cracking (mid-span)
	Damage 2	82%	Diagonal crack initiation on the right span
	Damage 3	96%	Extended diagonal cracking on the right span
	Damage 4	11% (after V_u)	Total failure (critical shear crack on the left span)
A0a	Damage 1	57%	Flexural cracking (mid-span)
	Damage 2	81%	Diagonal crack initiation on the left span
	Damage 3	96%	Diagonal cracking on the right span
	Damage 4	100% (=V_u)	Max shear strength (critical crack on the left span)
C0	Damage 1	60%	Flexural cracking (mid-span)
	Damage 2	80%	Diagonal crack initiation on the left span
	Damage 3	94%	Extended diagonal cracking on the left span
	Damage 4	34% (after V_u)	Total failure (critical shear crack on the right span)
C150	Damage 1	81%	Diagonal crack initiation on the left span
	Damage 2	92% (=V_{cr})	Extended diagonal cracking on the left span
	Damage 3	94% (after V_{cr})	Severe shear crack on the left span (stirrup yields)
	Damage 4	69% (after V_u)	Total failure (critical shear crack on the left span)
C225	Damage 1	87% (≅V_{cr})	Diagonal crack initiation on the left span
	Damage 2	63% (after V_{cr})	Extended diagonal cracking on the left span
	Damage 3	97% (≅V_u)	Severe shear crack on the left span (stirrup yields)

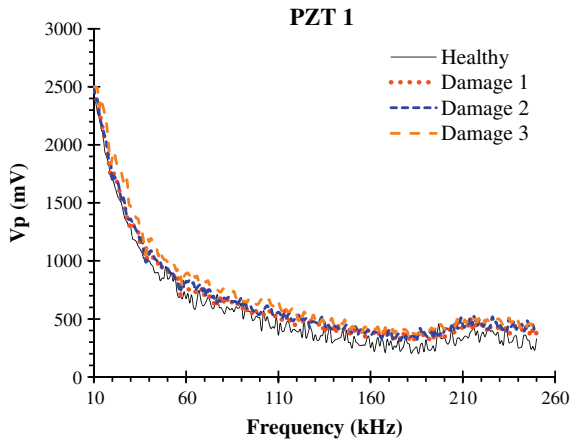

Fig. 10. Comparisons of the embedded "smart aggregate" transducer PZT1 of the beam A0 voltage signal measurements between the healthy state and the examined damage levels.

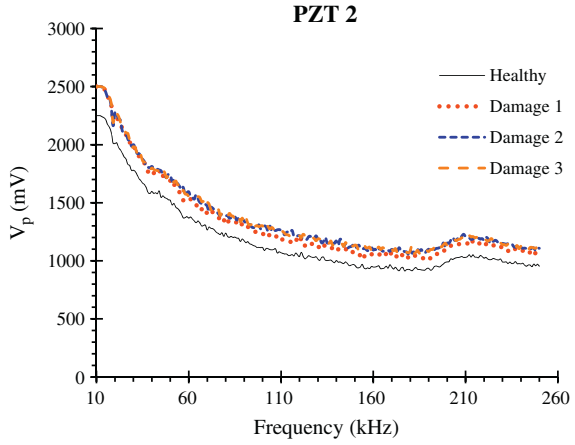

Fig. 11. Comparisons of the embedded "smart aggregate" transducer PZT2 of the beam A0 voltage signal measurements between the healthy state and the examined damage levels.

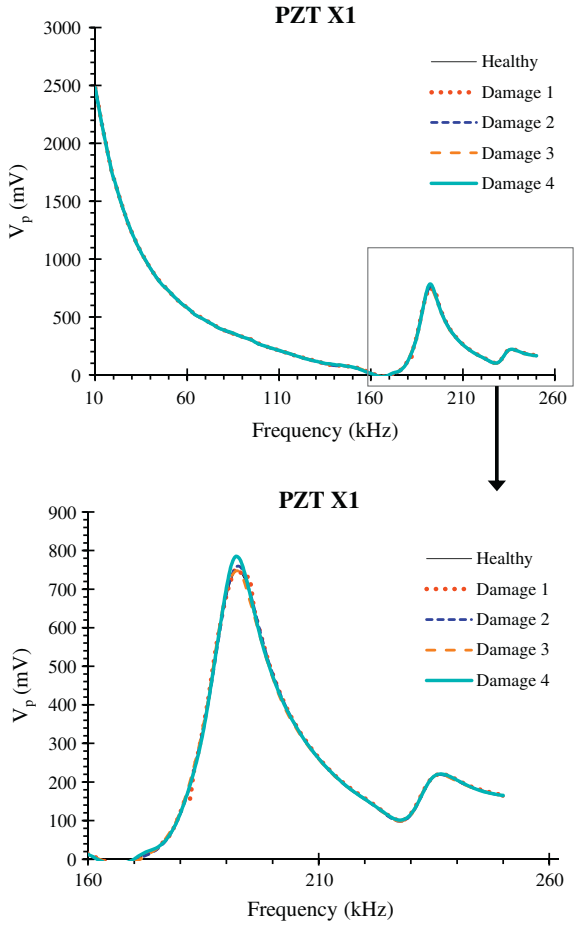

Fig. 12. Comparisons of the externally epoxy bonded transducer PZTX1 of the beam A0 voltage signal measurements between the healthy state and the examined damage levels.

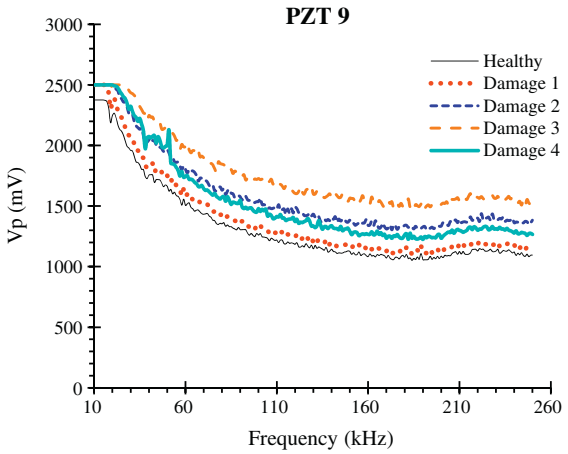

Fig. 13. Comparisons of the embedded "smart aggregate" transducer PZT9 measurements of voltage signal between the healthy state and the four damage levels of the beam C0.

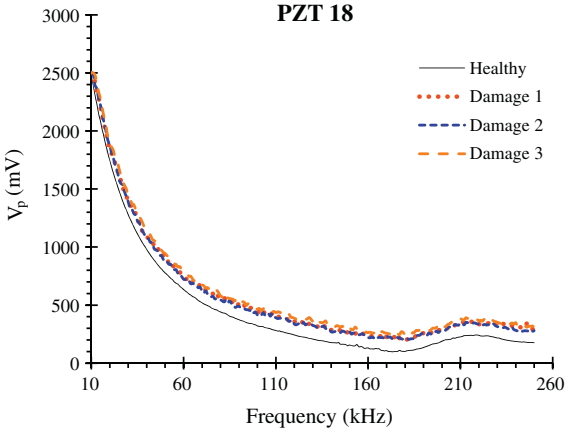

Fig. 14. Comparisons of the embedded "smart aggregate" transducer PZT18 measurements of voltage signal between the healthy state and the four damage levels of the beam C225.

number of measurements (the frequency index of each sum ranges from 10 kHz to 260 kHz).

Based on the adopted EMA technique principals, when damage occurred in any RC beam the voltage signal curves measured before damage (initial "Healthy" state) and after damage will change. The greater the damage, the greater the change in the voltage signal curves and, based on expression (8), the greater the absolute value of RMSD. Thus, RMSD index can be used to evaluate the evolvement of damage severity [56–58].

The frequency band of 10–260 kHz is selected for both embedded and surface bonded piezoelectric transducers for comparison reasons. However, Park et al. [59] indicated that the admittance signature of the PZT is significantly influenced by the constraint conditions and the degrees of freedom of the transducer that is mounted to the structural element. Thus, the different blocked conditions between the embedded and the surface bonded PZTs cause shifts in the slope and the pattern of the voltage versus frequency curves, as can be observed in Figs. 10–18. This fact could lead to the selection of different frequency bands for the calculation of RMSD index. Nevertheless, since there are discrepancies between the healthy and the damage states through the entire band of 10–260 kHz for both types of piezoelectric transducers, the same frequency band has been selected.

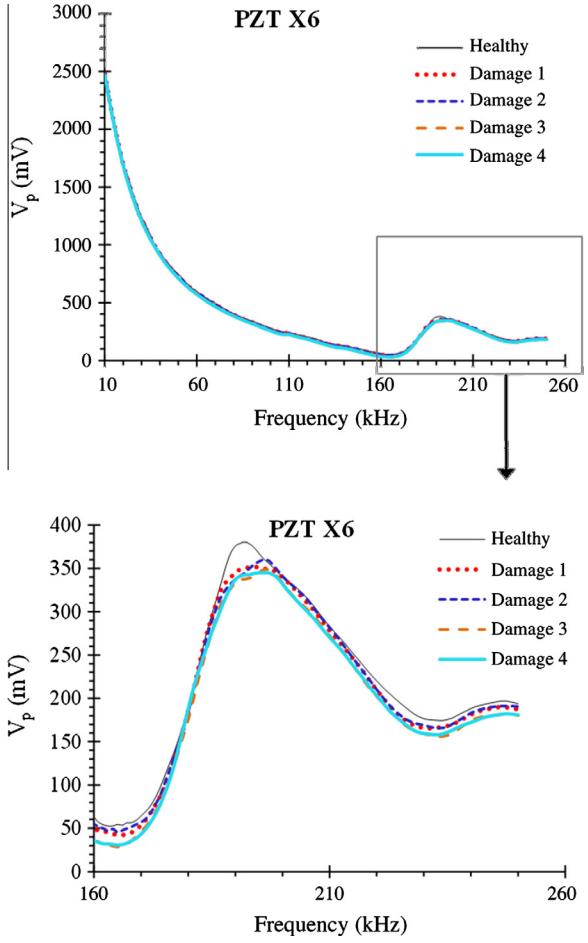

Fig. 15. Comparisons of the externally epoxy bonded transducer PZTX6 measurements of voltage signal between the healthy state and the four damage levels of the beam A0a.

Fig. 19a and b shows the histogram of RMSD index values for the voltage signal measurements of the epoxy bonded patches and the embedded "smart aggregate" transducers, respectively, for the examined damage levels of beam A0. In the same way, Figs. 20, 21, 22 and 23 display the histogram of RMSD index values for the voltage signal measurements of all PZTs mounted to beams A0a, C0, C150 and C225, respectively, for the examined damage levels.

It is noticeable that, more or less, along with the increase of the damage level, the values of RMSD calculated from the voltage signal measurements are rationally trending upwards in most of the mounted PZTs confirming the increased damage severity. Further, PZTs that exhibit low or decreased RMSD values at high damage levels indicate low or negligible damage severity in the concrete region that they are located. Thus, comparisons of the RMSD values derived from an array of PZTs mounted to specific positions of the examined RC beam can locate the locus and the magnitude of the occurred damage at different loading/damage levels, such as flexural cracking initiation, onset of diagonal crack, extended/severe diagonal cracking and final shear failure.

The aforementioned remarks are justified by the following observations and mainly from the measurements of the beams with stirrups (beams C150 and C225). In Fig. 22a the RMSD values of externally bonded patch PZTX13 are higher than the corresponding RMSD values of PZTX14 and it concludes that structural damage of beam C150 is occurred near PZTX13. This can be confirmed from the cracking patterns of beam C150 at each damage

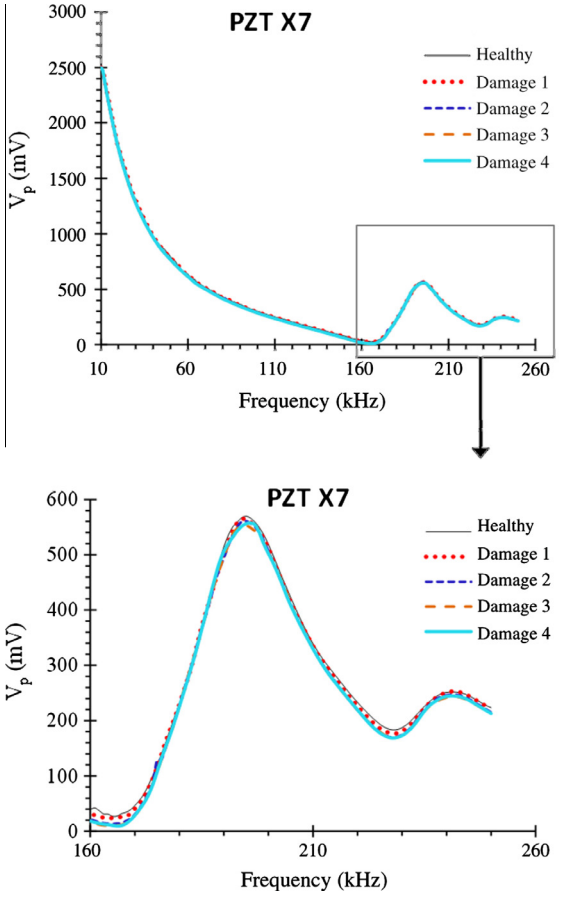

Fig. 16. Comparisons of the externally epoxy bonded transducer PZTX7 measurements of voltage signal between the healthy state and the four damage levels of the RC beam A0a.

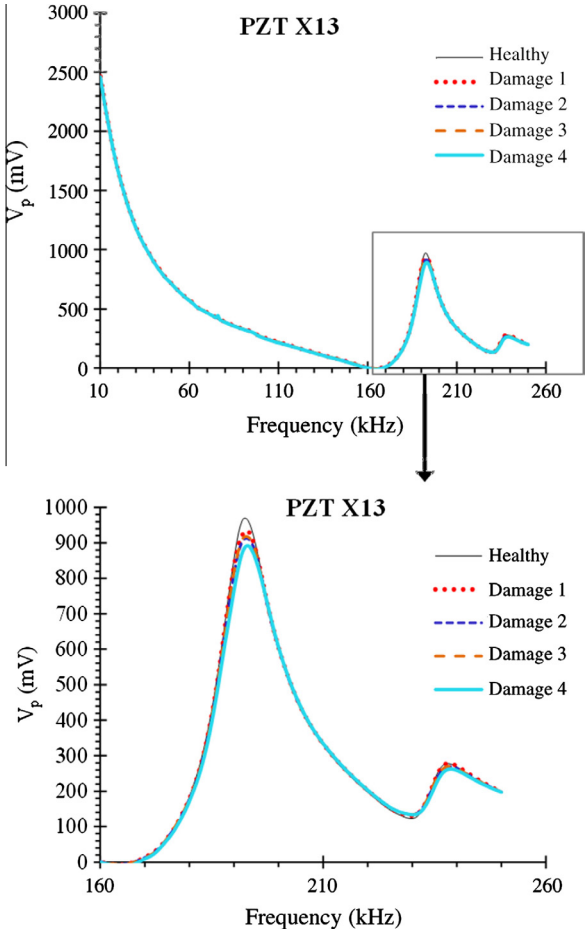

Fig. 17. Comparisons of the externally epoxy bonded transducer PZTX13 measurements of voltage signal between the healthy state and the four damage levels of the beam C150.

level shown in Fig. 8. The same conclusion can also be derived from the RMSD values of the embedded "smart aggregates" transducers PZT13 and PZT14 of beam C150 presented in Fig. 22b.

In the same way, RMSD values of the externally bonded patches PZTX17 and PZTX18 (Fig. 23a) and the embedded "smart aggregate" transducers PZT17, PZT18 and PZT19 (Fig. 23b) of beam C225 can locate the locus and the magnitude of the occurred damage at the examined loading and damage levels, as explained below:

- At Damage "1" (onset of diagonal crack) PZTX17 and PZT17 mounted to the left shear span of beam C225 exhibits slightly higher RMSD values than PZTX18 and PZT18 mounted to the right shear span, where a thin diagonal crack is initially occurred on the left shear span of the beam (see also cracking pattern (b) in Fig. 9). It is also noted that PZT19 that is placed near to the right support (right shear span) is far from the first diagonal crack and rationally its RMSD value is significantly low.
- At Damage "2" (extended diagonal cracking) PZT transducers of the left span (PZTX17 and PZT17) exhibits consistently higher RMSD values than PZTs of the right span (PZTX18, PZT18 and PZT19) and diagonal cracking is also extended on the left span of the beam as it can be shown in cracking pattern (c) of Fig. 9.
- At Damage "3", a severe shear crack has been developed on the left shear span (see also cracking pattern (d) in Fig. 9) and RMSD value of PZTX17 on the left span is significantly higher than the RMSD value of PZTX18 on the right span, ensuring (or predicting) this way that the final shear failure would inevitably be occurred on the left span as it actually happened and it can be observed in cracking pattern (e) of Fig. 9. It is emphasized that RMSD of PZT19 stayed in very low values during the test (see also Fig. 23b) since the region that it has been placed remained undamaged.

Although RMSD values of PZTs mounted to the shear-critical beams with stirrups (beams C150 and C225) provided sound indications of damage presence, location and evaluation, RMSD values of PZTs mounted to the beams without web reinforcement (beams A0 and C0) can hardly quantify damage assessment. This might be attributed to the fact that diagonal crack initiation occurred at one shear span (right span for beam A0 and left span for beam C0) whereas final diagonal shear crack formed at the other (left span for beam A0 and right span for beam C0). Nevertheless, there are several rational indications. RMSD values of the embedded "smart aggregate" transducers PZT1 and PZT2 that are placed on the left span of beam A0 are higher than the RMSD values of PZT3 and PZT4 that are placed on the right span of beam A0, where final shear crack formed at the left span (see also Figs. 19b and 5). Further, it is noted that RMSD values of PZT4 that is placed near to the right support and far from the diagonal damage occurred are relatively low since the region that it has been placed remained more or less undamaged. Further, by comparing the RMSD values of PZTX9 and PZTX10 of beam C0 (Fig. 21a) it can be found that the presence and growth of damage at each loading level cause a relative increase of the RMSD value of the transducer nearest to the damage.

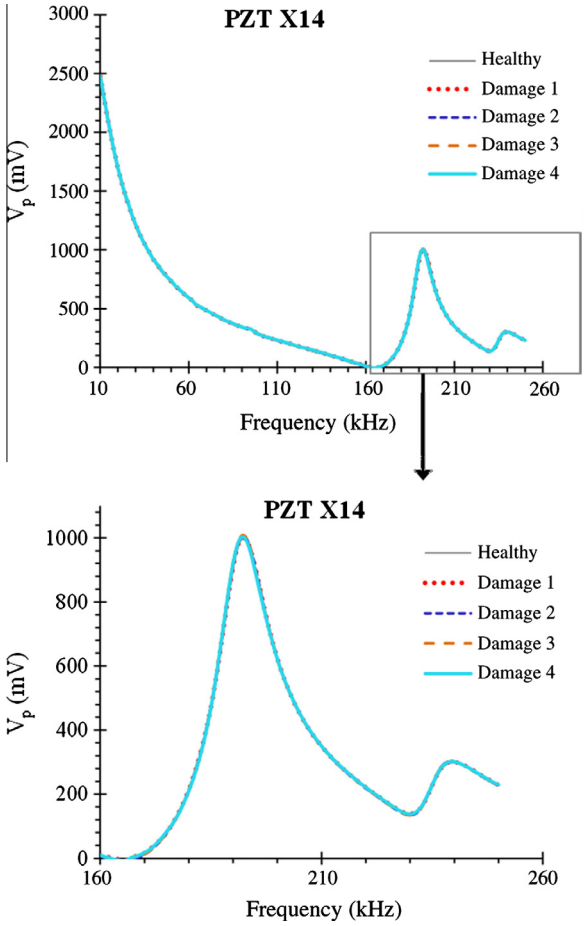

Fig. 18. Comparisons of the externally epoxy bonded transducer PZTX14 measurements of voltage signal between the healthy state and the four damage levels of the beam C150.

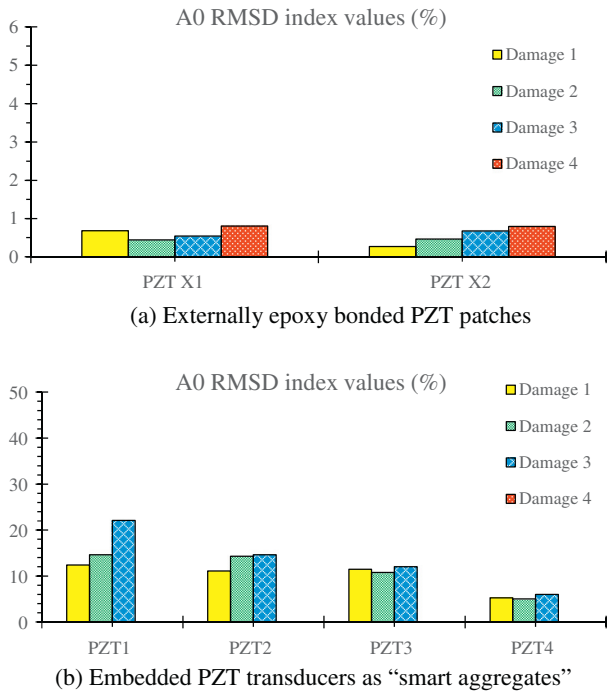

Fig. 19. RMSD index values for voltage signal measurements of the PZTs mounted to the beam A0 for the examined damage levels.

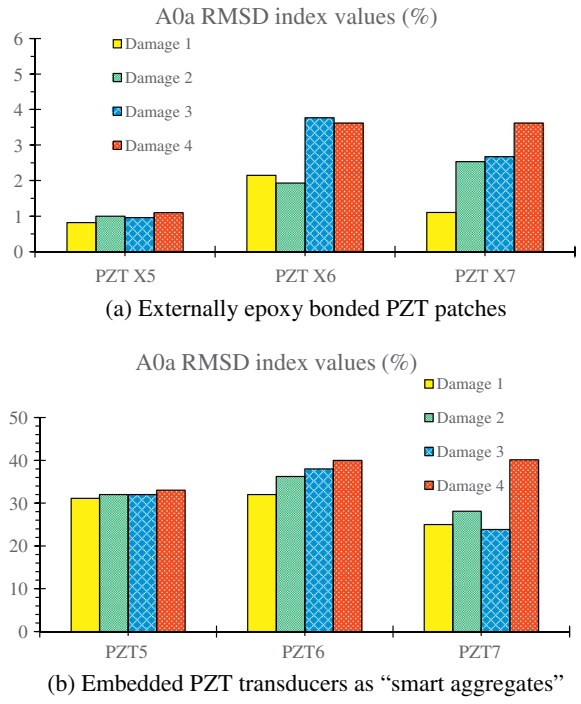

Fig. 20. RMSD index values for voltage signal measurements of the PZTs mounted to the beam A0a for the examined damage levels.

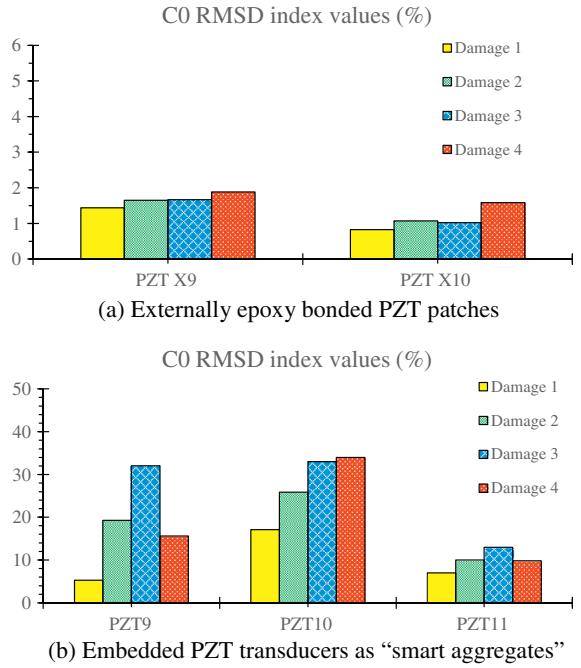

Fig. 21. RMSD index values for voltage signal measurements of the PZTs mounted to the beam C0 for the examined damage levels.

In Fig. 20a and b, RMSD values of all PZTs mounted to the left span of beam A0a, which is the critical shear span without web reinforcement where shear diagonal failure occurred, showed that along with the increase of the examined damage level the RMSD values are rationally and consistently increase. Further, PZTX5 exhibited lower RMSD values since it has been placed near the support and far farther from cracking with respect to the other PZTs of

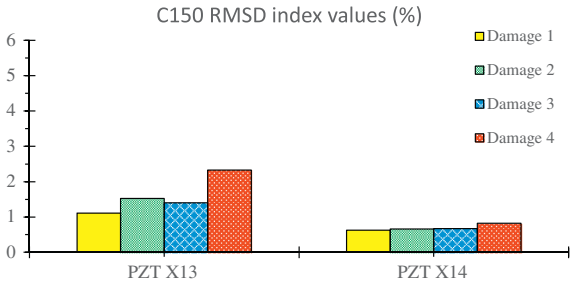

(a) Externally epoxy bonded PZT patches

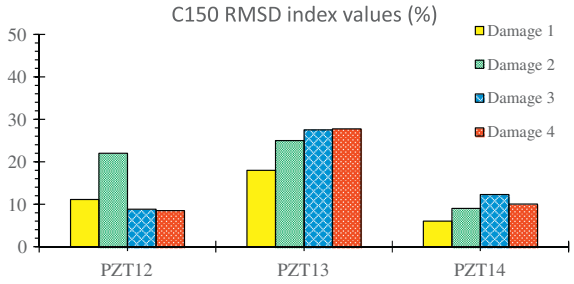

(b) Embedded PZT transducers as "smart aggregates"

Fig. 22. RMSD index values for voltage signal measurements of the PZTs mounted to the beam C150 for the examined damage levels.

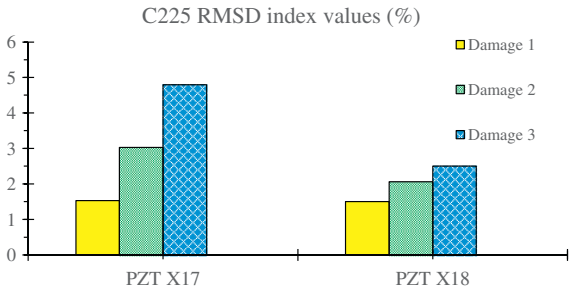

(a) Externally epoxy bonded PZT patches

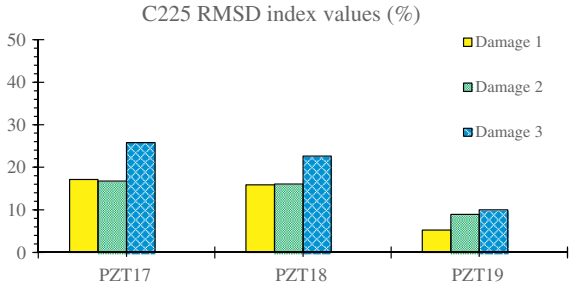

(b) Embedded PZT transducers as "smart aggregates"

Fig. 23. RMSD index values for voltage signal measurements of the PZTs mounted to the beam C225 for the examined damage levels.

the beam. RMSD values of the array of the externally bonded piezoelectric patches and the embedded "smart aggregate" transducers seem to provide satisfactory reliability for damage severity evaluation of the shear-critical RC beam and for the examined loading/damage levels. Although the obvious limitation of the pre-installation of embedded piezoelectric transducers prior concrete casting, the developed monitoring technique using the RMSD values of multiple surface bonded piezoelectric patches could successfully be applied in existing structures.

5. Conclusions

The ability of a new integrated wireless structural health monitoring system (WiAMS) to detect and evaluate damage severity level in shear-critical RC beams using voltage signatures of specially mounted piezoelectric transducers has been experimentally investigated. Two different settings of PZTs have been examined; (a) embedded piezoelectric transducers that have been pre-installed inside the beams as "smart aggregates" before concrete casting and (b) external piezoelectric patches that have been epoxy bonded on the surface of the beams in specific places across the potential diagonal cracking.

Voltage signatures of the piezoelectric transducers acquired from test measurements using WiAMS devices showed obvious discrepancies between the response of the healthy and the examined damage levels for every beam. These differences clearly indicate the presence of damage, whereas their gradual character reveals the magnitude of the occurred damage.

Damage assessment has been successfully attempted using values of the known statistical RMSD index. It has been found that along with the increase of the damage level, the values of RMSD calculated from the voltage signal measurements of the PZTs are rationally trending upwards confirming the increase of the damage severity. Both embedded and externally bonded transducers signals exhibited such response.

Comparisons of the RMSD values derived from an array of PZTs mounted to the beams can estimate the locus and the magnitude of the occurred damage at different loading/damage levels, such as flexural cracking initiation, onset of diagonal crack, extended/severe diagonal cracking and final shear failure. Further, in beams with stirrups, RMSD values of the PZTs mounted to the critical span where final shear failure occurred were remarkably higher than the corresponding values of the PZTs mounted to the other shear span of the beam. The above observations provide promising indications that the WiAMS measurements of a series of piezoelectric transducers mounted to specific locations of a shear-critical element could help to diagnose damage and to predict the forthcoming total shear failure at early damage stages, such as at the onset of diagonal cracking.

Acknowledgements

The contribution of the personnel of the Reinforced Concrete Laboratory in Democritus University of Thrace, Greece and especially the support and guidance of Professor C.G. Karayannis is greatly appreciated.

This research has been co-financed by the European Union (European Social Fund-ESF) and Greek National Funds through the Operational Programme "Education and Lifelong Learning" of the National Strategic Reference Framework (NSRF) – Research Funding Program: THALES. Investing in knowledge society through the European Social Fund.

References

[1] Chalioris CE, Favvata MJ, Karayannis CG. Reinforced concrete beam–column joints with crossed inclined bars under cyclic deformations. Earthq Eng Struct Dyn 2008;37(6):881–97.
[2] Favvata MJ, Karayannis CG, Liolios AA. Influence of exterior joint effect on the inter-story pounding interaction of structures. Struct Eng Mech 2009;33(2):113–36.
[3] Tsonos A-DG. A new method for earthquake strengthening of old R/C structures without the use of conventional reinforcement. Struct Eng Mech 2014;52(2):391–403.
[4] Divsholi BS, Yang Y, Bing L. Monitoring beam–column joint in concrete structures using piezo-impedance sensors. Adv Mater Res 2009;79–82:59–62.
[5] Park S, Kim J-W, Lee C, Park S-K. Impedance-based wireless debonding condition monitoring of CFRP laminated concrete structures. NDT&E Int 2011;44:232–8.

[6] Soh CK, Tseng KK-H, Bhalla S, Gupta A. Performance of smart piezoceramic patches in health monitoring of a RC bridge. Smart Mater Struct 2000;9(4):533–42.
[7] Yang Y, Miao A. Effect of external vibration on PZT impedance signature. Sensors 2008;8(11):6846–59.
[8] Shanker R, Bhalla S, Gupta A, Kumar MP. Dual use of PZT patches as sensors in global dynamic and local electromechanical impedance techniques for structural health monitoring. J Intell Mater Syst Struct 2011;22(16):1841–56.
[9] Wang D, Song H, Zhu H. Numerical and experimental studies on damage detection of a concrete beam based on PZT admittances and correlation coefficient. Constr Build Mater 2013;49:564–74.
[10] Liang C, Sun FP, Rogers CA. Coupled electromechanical analysis of adaptive material systems – determination of the actuator power consumption and system energy transfer. J Intell Mater Syst Struct 1994;5(1):12–20.
[11] Providakis CP, Karayannis CG, Chalioris CE, Favvata MJ, Angeli GM, Papadopoulos NA. Usage of PZTs for damage evaluation of steel reinforcing bar. Sch J Eng Technol 2015;3(1B):80–93.
[12] Divsholi BS, Yang Y. Application of PZT sensors for detection of damage severity and location in concrete. In: Proceedings of the SPIE. The International Society for Optical Engineering; 2008. p. 726813. http://dx.doi.org/10.1117/12.810696.
[13] Yang Y, Hu Y, Lu Y. Sensitivity of PZT impedance sensors for damage detection of concrete structures. Sensors 2008;8(1):327–46.
[14] Tawie R, Lee HK. Piezoelectric-based non-destructive monitoring of hydration of reinforced concrete as an indicator of bond development at the steel–concrete interface. Cem Concr Res 2010;40(12):1697–703.
[15] Providakis CP, Voutetaki ME, Seismic damage detection using smart piezo-transducers and electromechanical impedance signatures. In: Proceedings of the first European conference on earthquake engineering and seismology, 2006, Geneva, Switzerland; 2006. Paper number 307.
[16] Providakis CP, Voutetaki ME. Electromechanical admittance-based damage identification using Box–Behnken design of experiments. Struct Durab Health Monit 2007;3(4):211–27.
[17] Voutetaki ME, Providakis CP, Chalioris CE. FRP debonding prevention of strengthened concrete members under dynamic load using smart piezoelectric materials (PZT). In: Proceedings of the 15th European conference on composite materials, ECCM 2012 – composites at Venice, Venice, Italy; 2012. p. 24–8.
[18] Providakis CP, Stefanaki KD, Voutetaki ME, Tsompanakis J, Stavroulaki ME, Agadakos J. An integrated approach for structural health monitoring of concrete structures based on electromechanical admittance and guided waves. In: Proceedings of sixth ECCOMAS conference on smart structures and materials, Politecnico di Torino; 2013.
[19] Providakis CP, Stefanaki KD, Voutetaki ME, Tsompanakis J, Stavroulaki ME. Damage detection in concrete structures using a simultaneously activated multi-mode PZT active sensing system: numerical modelling. Struct Infrastruct Eng 2014;10(11):1451–68.
[20] Karayannis CG, Voutetaki ME, Chalioris CE, Providakis CP, Angeli GM. Detection of flexural damage stages for RC beams using piezoelectric sensors (PZT). Smart Struct Syst 2015;15(4).
[21] Talakokula V, Bhalla S, Gupta A. Corrosion assessment of reinforced concrete structures based on equivalent structural parameters using electro-mechanical impedance technique. J Intell Mater Syst Struct 2014;25(4):484–500.
[22] Providakis CP, Angeli GM, Favvata MJ, Papadopoulos NA, Chalioris CE, Karayannis CG. Detection of concrete reinforcement damage using piezoelectric materials – analytical and experimental study. Int J Civ Arch Struct Constr Eng 2014;8(2):197–205.
[23] Shin SW, Oh TK. Application of electro-mechanical impedance sensing technique for online monitoring of strength development in concrete using smart PZT patches. Constr Build Mater 2009;23(2):1185–8.
[24] Wang D, Zhu H. Monitoring of the strength gain of concrete using embedded PZT impedance transducer. Constr Build Mater 2011;25(9):3703–8.
[25] Providakis CP, Liarakos EV. T-WiEYE: an early-age concrete strength development monitoring and miniaturized wireless impedance sensing system. Proc Eng 2011;10:484–9.
[26] Providakis CP, Liarakos EV, Kampianakis E. Non-destructive wireless monitoring of early-age concrete strength gain using an innovative electromechanical impedance sensing system. Smart Mater Res 2013. 10 pgs 932568.
[27] Divsholi BS, Yang Y. Monitoring hydration of concrete with piezoelectric transducers. In: Proceedings of 35th conference on our world in concrete & structures, Singapore; 25–27 August 2010. Article online Id: 100035006.
[28] Song G, Gu H, Mo YL. Smart aggregates: multi-functional sensors for concrete structures – a tutorial and a review. Smart Mater Struct 2008;17(3):033001.
[29] Song G, Gu H, Mo YL, Hsu TTC, Dhonde H. Concrete structural health monitoring using embedded piezoceramic transducers. Smart Mater Struct 2007;16:959–68.
[30] Divsholi BS, Yang Y. Combined embedded and surface-bonded piezoelectric transducers for monitoring of concrete structures. NDT&E Int 2014;65:28–34.
[31] Kaur N, Bhalla S. Combined energy harvesting and structural health monitoring potential of embedded piezo-concrete vibration sensors. J Energy Eng ASCE 2014:D4014001. http://dx.doi.org/10.1061/(ASCE)EY.1943-7897.0000224.
[32] Kaur N, Bhalla S, Shanker R, Panigrahi R. Experimental evaluation of miniature impedance chip for structural health monitoring of prototype steel/RC structures. Exp Tech 2015. http://dx.doi.org/10.1111/ext.12146.
[33] Min J-Y, Park S, Yun C-B, Song B-H. Development of a low-cost multifunctional wireless impedance sensor node. Smart Struct Syst 2010;6(5):689–709.
[34] Nguyen K-D, Kim J-T. Smart PZT-interface for wireless impedance-based prestress-loss monitoring in tendon-anchorage connection. Smart Struct Syst 2012;9(6):489–504.
[35] Hou S, Yu Y, Zhang HB, Mao XQ, Ou JP. A SA-based wireless seismic stress monitoring system for concrete structures. Int J Distrib Sensor Networks 2013. http://dx.doi.org/10.1155/2013/978313. 7 pages 978313.
[36] Providakis CP, Liarakos EV. Web-based concrete strengthening monitoring using an innovative electromechanical impedance telemetric system and extreme values statistics. Struct Contr Health Monit 2014;21(9):1252–68.
[37] Providakis CP, Tsistrakis S, Voutetaki ME, Tsompanakis J, Stavroulaki M, Agadakos J, Kampianakis E, Pentes G. A wireless structural health monitoring system for damage detection in concrete structures based on an electromechanical impedance-type approach. In: 16th international conference & exhibition on "European Bridge Conference & Exhibition", Edinburgh, Scotland, UK; 23–25 June 2015.
[38] Chalioris CE, Providakis CP, Favvata MJ, Papadopoulos NA, Angeli GM, Karayannis CG. Experimental application of a wireless earthquake damage monitoring system (WiAMS) using PZT transducers in reinforced concrete beams. In: Proceedings of 10th international conference on earthquake resistant engineering structures (ERES 2015), Opatija, Croatia; 29 June – 1 July 2015.
[39] Kotsovos MD. Shear failure of reinforced concrete beams. J Eng Struct 1987;9(1):32–8.
[40] Zararis PD, Papadakis GC. Diagonal shear failure and size effect in RC beams without web reinforcement. J Struct Eng ASCE 2001;127:733–42.
[41] Ribas C, Cladera A. Experimental study on shear strength of beam-and-block floors. Eng Struct 2013;57:428–42.
[42] Chalioris CE. Steel fibrous RC beams subjected to cyclic deformations under predominant shear. Eng Struct 2013;49:104–18.
[43] Marí AR, Cladera A, Bairán J, Oller E, Ribas C. Shear-flexural strength mechanical model for the design and assessment of reinforced concrete beams subjected to point or distributed loads. Front Struct Civil Eng 2014;8(4):337–53.
[44] Karayannis CG, Chalioris CE. Shear tests of reinforced concrete beams with continuous rectangular spiral reinforcement. Constr Build Mater 2013;46:86–97.
[45] Cladera A, Marí AR. Shear strength in the new Eurocode 2. A step forward? Struct Concr 2007;8(2):57–66.
[46] Cladera A, Marí A, Ribas C, Bairán J, Oller E. Predicting the shear-flexural strength of slender reinforced concrete T and I shaped beams. Eng Struct 2015;101:386–98.
[47] Chalioris CE, Papadopoulos NA, Angeli GM, Karayannis CG, Liolios AA, Providakis CP. Damage evaluation in shear-critical reinforced concrete beam using piezoelectric transducers as smart aggregates. Open Eng 2015;5(1):373–84.
[48] Naidu ASK, Soh CK. Damage severity and propagation characterization with admittance signatures of piezo transducers. Smart Mater Struct 2004;13(2):393–403.
[49] Bhalla S, Soh CK. Structural health monitoring by piezo-impedance transducers I: modelling. J Aerospace Eng ASCE 2004;17(4):154–65.
[50] Providakis CP, Tsistrakis S, Voutetaki ME, Tsompanakis J, Stavroulaki M, Agadakos J, Kampianakis E, Pentes G. A new damage identification approach based on impedance-type measurements and 2D error statistics. Struct Monit Mainten 2015;2(4):319–38.
[51] Bhalla S, Soh CK. Electromechanical impedance modeling for adhesively bonded piezo-transducers. J Intell Mater Syst Struct 2004;15(12):955–72.
[52] Zhao J, Bao T, Chen S, Kundu T. Smart aggregate-piezoceramic patch combination for health monitoring of concrete structures. J Sensors 2016. 7pgs 3270916.
[53] Koo KY, Park S, Lee J-J, Yun C-B. Automated impedance-based structural health monitoring incorporating effective frequency shift for compensating temperature effects. J Intell Mater Syst Struct 2009;20:367–77.
[54] Hu X, Zhu H, Wang D. A study of concrete slab damage detection based on the electromechanical impedance method. Sensors 2014;14(10):19897–909.
[55] Giurgiutiu V, Reynolds A, Rogers CA. Experimental investigation of E/M impedance health monitoring for spot-welded structural joints. J Intell Mater Syst Struct 1999;10(10):802–12.
[56] Xu D, Cheng X, Huang S, Jiang M. Identifying technology for structural damage based on the impedance analysis of piezoelectric sensor. Constr Build Mater 2010;24(12):2522–7.
[57] Bhalla S, Vittal APR, Veljkovic M. Piezo-impedance transducers for residual fatigue life assessment of bolted steel joints. J Struct Health Monit 2012;11(6):733–50.
[58] Tseng K, Naidu A. Non-parametric damage detection and characterization using smart piezoceramic materials. Smart Mater Struct 2002;11:317–29.
[59] Park G, Farrar CR, Scalea FL, Coccia S. Performance assessment and validation of piezoelectric active-sensors in structural health monitoring. Smart Mater Struct 2006;15(6):1673–83.